Supramolecular-Templated Thick Mesoporous Titania Films for Dye-Sensitized Solar Cells: Effect of Morphology on Performance

Yu Zhang, Zhibin Xie, and John Wang*

Department of Materials Science and Engineering, National University of Singapore, Singapore 117576

ABSTRACT Highly crystallized mesoporous titania films of varying thicknesses and different morphologies, namely ordered body-centered orthorhombic and disordered wormlike mesostructure, have been successfully synthesized via a supramolecular-templated route and subsequent layer-by-layer deposition. The performance of these mesoporous films in dye-sensitized solar cells was investigated, achieving a maximum efficiency of 6−7% at the film thickness of 5−6 μm. The ordered mesoporous titania films outperformed the disordered counterpart of the same thickness in both short circuit current and efficiency. This behavior is elaborated with the dye-loading, optical, and charge-transport behavior as affected by the variation in mesoporous film morphology. The improved cell performance of the ordered mesoporous film is ascribed to the enhanced electron transport in the regularly packed titania network because of the enhanced crystalline grain connectivity. Nevertheless, the dependence of cell performance on the film morphology is weakened when the film thickness was above ~3.5 μm, because of the serious film cracks.

KEYWORDS: dye-sensitized solar cells • supramolecular-templated • mesoporous • morphology • titania

1. INTRODUCTION

Dye-sensitized solar cells (DSSCs) have long been regarded as a promising alternative to conventional solid-state semiconductor solar cells, on the basis of their relatively high efficiency over 10% at a very competitively low cost (1−3). However, further increasing the energy conversion efficiency of DSSCs remains a technological challenge. The main bottleneck lies in the dynamic competition between electron transport in the conduction band of semiconductor oxide and the interfacial recombination of charge carriers at the semiconductor oxide/electrolyte interfaces (4). In this regard, efforts in modifying the semiconductor structure to speed up the electron transport and at the same time to slow down electron recombination are crucial but yet successful (5, 6). Currently, the most efficient semiconductors as the photoanode are typically composed of randomly clustered titania nanoparticles 15−20 nm in size, forming a three-dimensional network with a layer thickness of 10−15 μm (1−3). However, transporting electrons through these titania nanoparticles would not be efficient, because the electrons have to pass through numerous grain boundaries and junctions in order to reach the transparent conductive oxide (TCO) (7, 8). The distortion of the crystalline structure at grain boundaries and junctions may lead to enhanced scattering of electrons with the lattice and hence to a reduced electron mobility. One possible solution is to use one-dimensional nanostructures such as the standing nanorods, nanowires, or nanotubes that are able to provide direct pathways for electron transport through the device thickness and therefore reduce the degree of charge recombination. However, such one-dimensional nanostructures have insufficiently high internal surface area to adsorb dye molecules, which greatly limits their optical absorption efficiency and thus energy conversion efficiency at a relatively low level (9).

Consequently, both charge transport/recombination kinetics and surface area of the semiconductors are the key parameters determining their effectiveness in solar cell device applications (10). These parameters, on the one hand, are determined by the nanostructural parameters of the semiconductor such as the crystallinity, crystallite size, defect type and concentration, and impurities; on the other hand, they are also strongly affected by the film morphology of the semiconductor photoanode. Supramolecular-templated mesoporous titania thick films have therefore attracted increasing interest as photoanodes in DSSCs, because of their continuous and tunable mesoporous structures with large specific surface area, interconnected titania skeleton with regular nanocrystal junctions, and the ability to develop a range of controlled morphologies.

Nevertheless, for the supramolecular-templated mesoporous titania films, only limited success in the device performance has been achieved thus far, as a result of the combination of several unsolved technical issues. Supramolecular-templated titania films often exhibit a semicrystalline network with the coexistence of anatase nanocrystals and a significant amount of amorphous titania. The low crystallinity always causes low solar conversion efficiencies (<1.25%) (11, 12). Several approaches have been attempted to increase the nanocrystallinity whereas to preserve the porous structure, such as by using block-copolymers to template

* To whom correspondence should be addressed. Phone: +65 65161268. Fax: +65 67763604. E-mail: msewangj@nus.edu.sg.
Received for review August 10, 2009 and accepted November 9, 2009

DOI: 10.1021/am900529e

hydrothermally synthesized anatase seeds (13), employing a two-step sintering procedure (12), and doping phosphorus in titania (14). DSSC conversion efficiencies of 2.2−5.35% were reported (12−14). However, the mesostructures that were formed in these titania films lacked a long-range ordering, and the titania nanoparticles were still randomly interconnected forming an irregular inorganic framework. DSSC photoanodes with ordered cubical mesoporous titania films of ~1 μm in thickness were attempted, through layer-by-layer deposition by dip coating three times (15). They showed a solar conversion efficiency in the range of 2.95 and 4.04%, higher than those of the conventional oxide films of similar thickness made of randomly clustered anatase nanocrystals. The cell performance of thick mesoporous films with ordered mesostructure has however not been reported, probably because of the poor pore accessibility associated with the thick film that limits the dye adsorption and the electrolyte percolation (16).

In this work, ordered mesoporous titania films several micrometers in thickness were successfully synthesized via a modified layer-by-layer deposition by spin-coating. Given that the supramolecular templating approach could produce a range of controlled morphologies in the same material system and on the same length scale, it offers an excellent platform for investigating the dependence of cell performance on the film morphology of TiO_2 mesolayers. We synthesized two supramolecular-templated mesoporous titania systems with similar nanostructures (crystalline phase, crystallite size, and roughness factor), but with completely different mesostructural morphologies, namely an ordered body-centered orthorhombic and a disordered wormlike mesostructure, by tuning the ratio of suparmolecular templates to titania species. These films were integrated in DSSCs, demonstrating a complex interplay of factors determining the cell performance. A high solar cell efficiency in the range of 6−7% was achieved at a film thickness of 5−6 μm. To the best of our knowledge, this represents the highest efficiency obtained by the photoanodes made of the supramolecular-templated mesoporous titania film.

2. EXPERIMENTAL SECTION

Preparation of Supramolecular-Templated Mesoporous Titania Films. A precursor solution was first prepared by mixing appropriate amounts of ethanol (99.8%), hydrochloric acid (HCl, 36%), titanium tetraisopropoxide (TTIP, 97%), acetyl acetone (AcAc, 99.5%), and deionized water (H_2O), and followed by stirring for 2 h. Triblock copolymer Pluronic F127 ($EO_{106}PO_{70}EO_{106}$) was dissolved in ethanol and then mixed with the precursor solution. Molar ratios of these ingredients were controlled as follows: TTIP/AcAc/HCl/H_2O/ethanol/F127 = 1:0.5:0.5:15:40:f (f = 0.005 or 0.01). After stirring for three more hours, the sol solution thus obtained was deposited on fluorine-doped tin oxide (FTO, TEC 15 from Dyesol, 3 mm thick, 80% transmittance in the visible, 15 Ω/sq) substrates by spin coating (2000 rpm for 1 min) at a relative humidity of 70%. The spin-coated film was exposed to ethanol vapor for 5 min at room temperature by dropping liquid ethanol on a filter paper surrounding the sample. The vapor treatment reduces the surface irregularity and lessens the strain in the film by slowing down the drying process. The film was then cured on a hot plate at 300 °C for 15 min in air to enhance the inorganic polymerization and to stabilize the mesophases involved. Repetitive spin-coatings, exposing to ethanol vapor, and curing were carried out until the desired film thickness was reached. Afterward, the film sample was calcined in air at 350 °C for 4 h (1 °C min^{-1} ramp) to remove the organic copolymer templates, and then thermally annealed at 450 °C for 1 h (1 °C min^{-1} ramp) to improve the nanocrystallinity of the mesoporous titania.

Fabrication of DSSCs. During the cooling process, the mesoporous titania film was immersed in anhydrous ethanol containing 5×10^{-4} M *cis*-bis(isothiocyanato)bis(2,2′-bipyridine-4,4′-dicarboxylato) ruthenium(II) bis-tetrabutylammonium (N719 dye, Solaronix), when it was still warm (80−100 °C), and kept at room temperature for 3 days. The dye-adsorbed electrode was then rinsed thoroughly with ethanol and dried. The Pt-coated FTO (Dyesol), which is employed as a counter electrode, was heated at 400 °C for 20 min in air before cell assembly. The electrolyte solution consisted of 0.6 M 1-butyl-3-methylimidazolium iodide (98%, Ionic Liquids Technology), 0.03 M iodine (99.5%), 0.1 M guanidine thiocyanate (99%), and 0.5 M 4-tert-butylpyridine (98%) in acetonitrile (99.8%)/valeronitrile (99.5%) (85/15, v/v). The electrodes were spaced and sealed by 25 μm thick thermoplast hot-melt sealing foil (SX1170−25, Solaronix). The electrolyte was introduced with the help of one hole in the Pt-coated FTO via vacuum backfilling, and the hole was then sealed using SX1170−25 film. The cells masked with black plastic tape had an active area of 0.5−0.7 cm^2.

Characterization. X-ray diffraction (XRD, Bruker AXS D8 Advance, Germany) measurements were carried out to identify the crystalline phase and crystallinity of titania present in the mesoporous films, by using Cu Kα radiation (1.5406 Å) operated at 40 kV and 40 mA with a step size of 0.02°, a time per step of 1 s, and 2θ range of 20−70°. Transmission electron microscopy (TEM, JEOL JEM 2010F, 200 kV) was employed to investigate the texture and morphology of the mesoporous films. For TEM studies, the sample was scratched off the substrate and then dispersed in ethanol, after which it was dropped and dried on a carbon-coated copper grid. Field emission scanning electron microscopy (SEM-FEG XL 30) was performed to characterize the film texture and thickness. The optical properties were measured by using a UV−vis NIR spectrophotometer (Varian Cary 500). FT-IR spectrophotometer (Varian 3100 Excalibur) was employed to identify the organic components in the titania films. The N_2 adsorption and desorption isotherms at −196 °C were measured using a Micromeritics ASAP 2020 system after the samples that were scratched off the substrate were degassed at 200 °C for 8 h. The Brunauer−Emmett−Teller (BET) surface area was estimated using adsorption data in a relative pressure range from 0.08 to 0.2. The total pore volume was calculated from the amount of N_2 adsorbed at a relative pressure of P/P_0 = 0.985. The pore size distribution was calculated by analyzing the desorption branch of the N_2 isotherm using the Barrett−Joyner−Halenda (BJH) method.

Photocurrent−voltage measurements of the cell samples were performed under a simulated AM 1.5 solar illumination at an intensity of 100 mW cm^{-2}, by using a Keithley 2420 sourcemeter. The irradiance source was a 150W NREL traceable Oriel Class AAA solar simulator (Model 92250A-1000). The output power was calibrated by a NREL traceable monocrystalline silicon reference cell (PVM 191) coupled with Newport Oriel PV reference cell system (model 91150). Incident photon-to-current conversion efficiency (IPCE) was measured by the DC method. The light source was a 300 W xenon Lamp (Oriel 6258) coupled with a flux controller to improve the stability of the irradiance. The light passed through a monochromator (Cornerstone 260 Oriel 74125) to select a single wavelength with a resolution of 10 nm. Light intensity was measured by a NREL traceable Si detector (Oriel 71030NS) and the short circuit currents of the DSSCs were measured by an optical power meter (Oriel 70310).

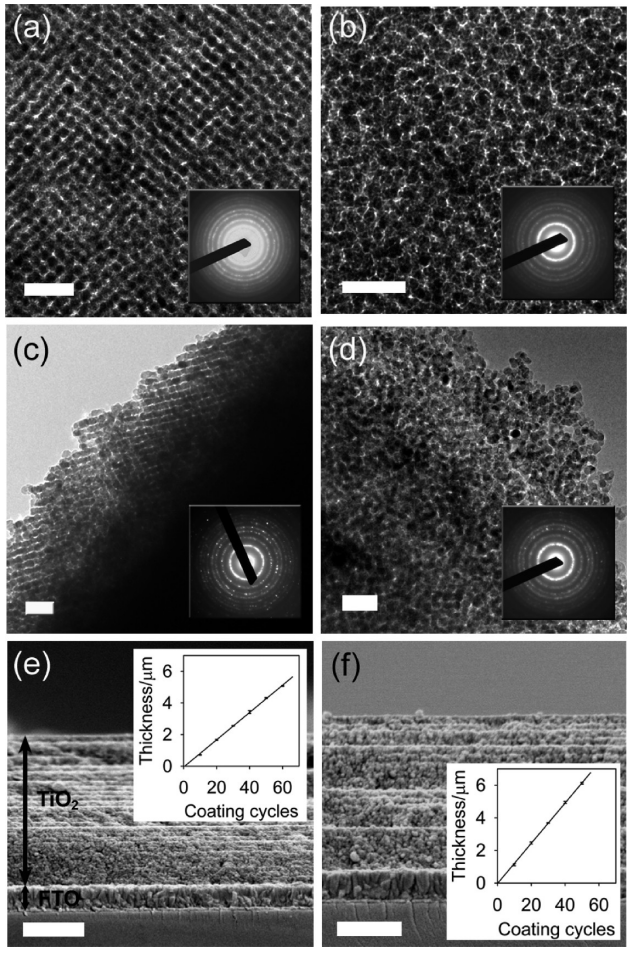

FIGURE 1. TEM images of the ordered body-centered orthorhombic mesoporous (a) one-layer (~85 nm) and (c) 2.5 μm thick titania films. TEM images of the disordered wormlike mesoporous (b) one-layer (~125 nm) and (d) 2.5 μm thick titania films. Insets in a–d are the corresponding selected area diffraction patterns. Scale bar for a–d: 50 nm. Cross-sectional SEM micrographs of the (e) ordered and (f) disordered mesoporous 2.5 μm thick titania films. Insets in e–f show the variation in film thickness with the spin-coating cycles. Scale bar for e–f: 1 μm.

3. RESULTS AND DISCUSSION

Structural Analysis of Mesoporous Titania Films of Different Morphologies. Supramolecular-templated mesoporous titania films of different morphologies were synthesized by delicately controlling the interactions between the templating molecules (Pluronic F127) and the inorganic species. Under the sol solution condition of TTIP/AcAc/HCl/H_2O/ethanol/F127 = 1:0.5:0.5:15:40:f (molar ratio), the deposited one-layer film showed either an ordered body-centered orthorhombic (Figure 1a) or a disordered wormlike (Figure 1b) mesostructure at f = 0.005 or 0.01, respectively, upon calcination at 450 °C. The mesostructure characterization was detailedly described in a previous study by using a combination of small-angle X-ray scattering, SEM and TEM techniques (17), where the ordered body-centered orthorhombic mesoporous structure was demonstrated to be oriented with the (001) plane parallel to the substrate and the lattice parameters of a, b, and c were evaluated to be 15.2, 26.4, and 10.0 nm, respectively.

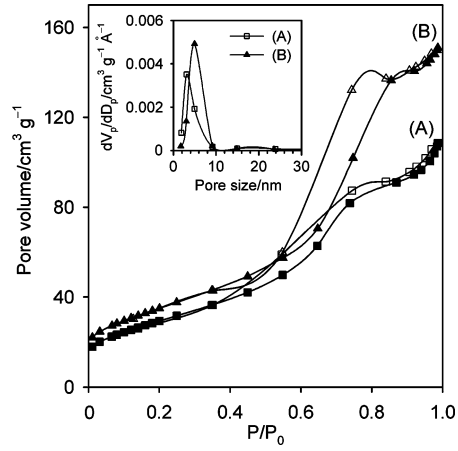

FIGURE 2. N_2 adsorption–desorption isotherms of the (A) ordered and (B) disordered mesoporous 2.5 μm thick titania films. Solid and open symbols denote adsorption and desorption branches, respectively. Inset: BJH pore size distributions calculated from the desorption branches of the N_2 isotherms.

Layer-by-layer deposition by spin-coating was then applied to form thick films up to micrometer scale. As shown by the TEM images of the multilayered 2.5 μm thick films (images c and d in Figure 1), the layer-by-layer deposition did not disturb the mesopore configuration significantly, which is consistent with the observation of other groups (15). The film thickness was linearly proportional to the coating cycles (insets of e and f in Figure 1), with a notable interface observed between each two neighboring layers (images e and f in Figure 1).

Figure 2 is the N_2 adsorption–desorption isotherms and pore size distributions of the mesoporous titania films of 2.5 μm in thickness. They are typical type *IV* isotherms. The monolayer adsorption was not complete until a relative pressure of ~0.4 was reached, where the loop opened, indicating the existence of mesopores. The BET surface areas for the ordered and the disordered mesoporous titania were calculated to be 107.7 and 127.2 $m^2 g^{-1}$, respectively, with the pore volume of 0.17 and 0.23 $cm^3 g^{-1}$, respectively. Narrow pore size distributions of 2–10 nm were calculated for both the ordered and disordered mesoporous titania films, by analyzing the desorption branches of the N_2 isotherms using the BJH method. They imply a mesoscopic textural gradient along the direction perpendicular to the substrate, with the layers close to the film/air surface featuring bigger pore size (~10 nm) than those close to the film/substrate interface (~2 nm), because the former underwent fewer thermal annealing cycles. The average pore sizes for the ordered and disordered mesoporous titania were calculated to be 4.5 and 5.1 nm, respectively. The increase in surface area, pore volume, and pore size for the disordered mesoporous titania than the ordered counterpart is ascribed to the fact that the former had a higher content of organic template, which constructed the pore space upon decomposition.

On the other hand, when the pore volume increases, the mass of titania decreases. The ordered mesoporous titania film with less pore volume thus possesses a higher titania weight than that of the disordered one of the same thickness. The roughness factor, which is the product of the specific

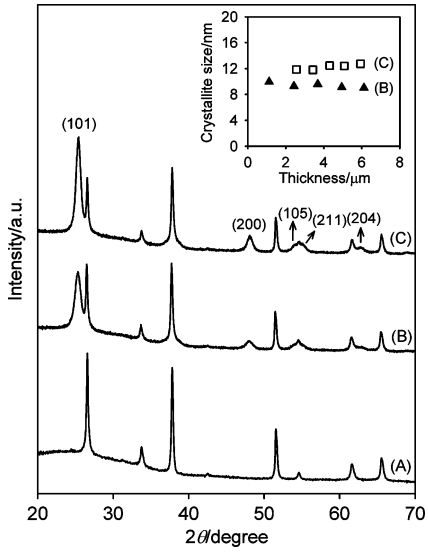

FIGURE 3. XRD patterns of the (A) FTO substrate, (B) disordered and (C) ordered mesoporous 2.5 μm thick titania films. The peaks in XRD patterns can be ascribed to the (101), (200), (105), (211), and (204) planes of the anatase phase, respectively. The unindexed diffraction peaks are ascribed to the FTO substrate. Inset is the variation of crystallite size with film thickness. The crystallite size was calculated by using the Scherrer equation by fitting the (101) diffraction peak of anatase to Lorentz distribution.

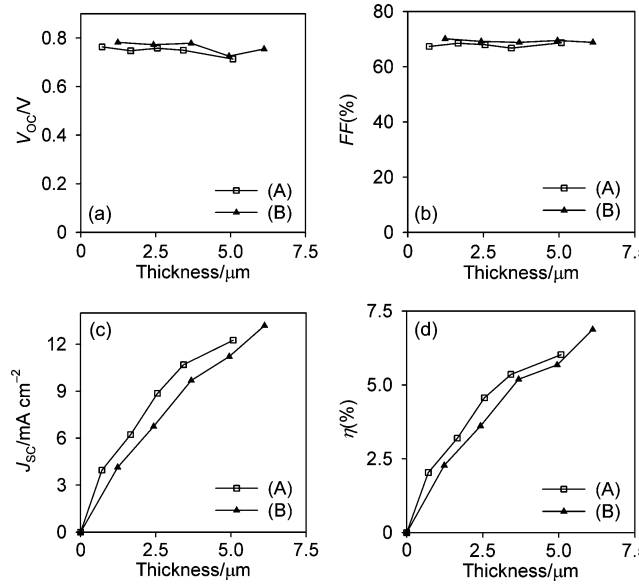

FIGURE 4. Solar cell performance comparison of the (A) ordered and (B) disordered mesoporous titania film DSSCs. All solar tests were operated under the simulated AM 1.5 solar illumination at an intensity of 100 mW cm^{-2}.

surface area and titania weight (18), is therefore almost identical for the ordered and the disordered mesoporous 2.5 μm thick titania film, with values of 181.9 and 180.5 μm^{-1}, respectively.

Both the ordered and disordered mesoporous titania films showed a high crystallinity, as evidenced by the well-established selected area diffraction (Figure 1a–d, insets) and XRD (Figure 3) patterns. The peaks in XRD patterns can be ascribed to the (101), (200), (105), (211), and (204) planes of the anatase phase, respectively. The crystallite size is calculated using the Scherrer equation by fitting the (101) peak of the anatase phase to Lorentz distribution. As shown by Figure 3 inset, the crystallite size is irrelative to the film thickness, attributed to the spatial confinement effect of mesopore arrays. The ordered mesoporous titania films showed a slightly larger crystallite size (~12 nm) than the disordered films (~9.5 nm). It suggests that the nanoparticles composing the mesoporous titania network as displayed in the TEM images (Figure 1a-d) are single crystals each. Again, the variation in crystallite size with morphology is attributed to the different level of supramolecular template content employed. As the ordered mesoporous titania film was synthesized under a lower template content, it possesses a higher titania content and therefore thicker titania walls than the disordered film. The thicker titania walls are capable of embracing relatively larger nanocrystals.

Influence of Mesostructural Morphologies on Photovoltaic Performance. The mesoporous titania films of different morphologies and thicknesses were studied for their performance as photoanodes in DSSCs, which are presented in Figure 4. It shows that, for both the ordered and the disordered mesoporous titania derived DSSCs, there were no remarkable changes in the open circuit voltage (V_{OC}) and the fill factor (*FF*) with the changes in film thickness and morphologies (panels a and b in Figure 4). In general, the V_{OC} is very sensitive to change in surface potential of titania, which is dependent upon defect density, location, impurities, and fabrication protocol (7). As the films investigated in the present work were fabricated in the same manner, it is reasonable to expect comparable trap densities and trap sites in both the ordered and the disordered mesoporous films. Consequently, there are no evident changes in the surface potential and henceby V_{OC}.

But the short circuit current density (J_{SC}) and the efficiency (η) were greatly affected by the film thickness and morphologies (panels c and d in Figure 4). It is the variation in J_{SC} that is mainly responsible for the change in the η. The J_{SC} increased with increasing film thickness, ascribed to an increase in total surface area with the increasing film thickness. More importantly, the ordered mesoporous titania photoanode achieved a higher J_{SC} than the disordered one of the same thickness, indicating the dependence of J_{SC} and thus η on the structural morphologies.

Desorption studies were performed where the N719-sensitized mesoporous titania film was thoroughly rinsed with ethanol before being immersed into excess NaOH (5 mL, 1 mM) for 1 h to desorb and fully deprotonate the dye (19). The absorbance of the resulting light pink solution was measured by using a UV–vis NIR spectrophotometer. The molar extinction coefficient of the fully deprotonated dye at 500 nm wavelength was measured to be $\varepsilon = 14850$ M^{-1} cm^{-1}; the dye loading was calculated according to the Beer's law. For both the ordered and disordered mesoporous titania films, the surface concentration (C_{surf}) of the dye on the film increased with increasing film thickness because of the increased surface area (Figure 5a). Interestingly, the ordered and disordered films of the same thickness have comparable degrees of dye loading, indicating an almost identical ac-

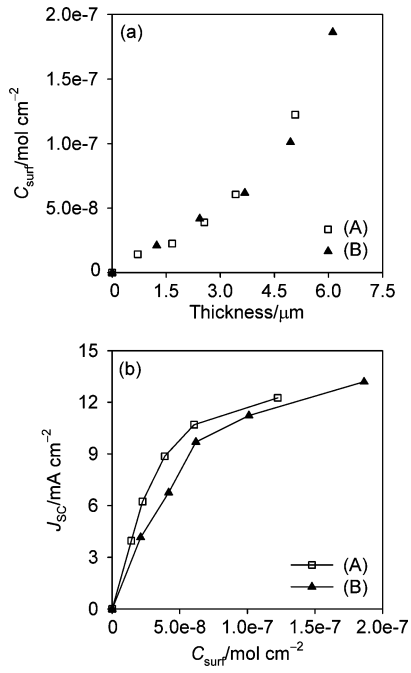

FIGURE 5. (a) Dye adsorption on the (A) ordered and (B) disordered mesoporous titania films of varying thicknesses. (b) The relationship between the J_{SC} and the dye loading for the (A) ordered and (B) disordered mesoporous titania films.

cessible area in the actual device geometry for dye uptake. This is consistent with the previous roughness factor analysis that the ordered and the disordered 2.5 μm thick films displayed almost equal values of roughness factors. It rules out the possibility that the difference in J_{SC} for the titania films of different morphologies arises from their different dye uptake abilities.

Careful observation revealed that the C_{surf} versus thickness plots presented an accelerated slope, indicating that the dye uptake increased in an accelerated manner with the film thickness. However, the added dye loading for thicker films did not equally give rise to an accelerated rise in current, as it was apparent from the decreased slopes for the J_{SC} versus the C_{surf} plots (Figure 5b). Approximately, the J_{SC} versus dye uptake plots can be divided into two regions. In region 1 (C_{surf} $< 6 \times 10^{-8}$ mol cm^{-2}, corresponding to the film thickness less than ~3.5 μm), the photocurrent of the cell increased almost linearly with the dye loading; this enhancement in current became less distinct in region 2 ($C_{surf} > 6 \times 10^{-8}$ mol cm^{-2}).

Such behavior is attributed to the formation and spatial distribution of cracks in the mesoporous films. We have observed that cracks gradually appeared in the titania film with increasing film thickness. Below the film thickness of ~3.5 μm, no or insignificant number of cracks was observed in the film. However, when the film was thicker than ~3.5 μm, large cracks were visible to the naked eyes. On the one hand, the presence of a large number of cracks in thicker films provides more surfaces for adsorbing dye molecules. On the other hand, these macro-cracks decrease the coordination number of TiO_2 nanocrystallites at the crack surface. The disconnected nanocrystallites give rise to a slow down in electron transport and an increase in recombination rate (20). In addition, the macro-cracks can increase the area of exposed FTO substrate, leading to an increase in current leakage. Consequently, the dye loading shows an accelerated increasing trend with the film thickness, but it does not contribute to the photocurrent increase when the charge carriers are annihilated at the recombination centers.

Additionally, in region 1, the DSSCs made of the ordered mesoporous titania films showed much higher photocurrent as compared to those of their disordered counterparts of identical dye loading. In region 2, the difference in current between the ordered and the disordered mesoporous titania photoanodes was diminished. Again, it is ascribed to the formation of macro-cracks in the thick films. At $C_{surf} > 6 \times 10^{-8}$ M, macro-cracks spread extensively through the thick films. They disrupt the structural order, inevitably attenuating the superiority of the ordered mesoporous titania in charge carrier transport, and blurring the difference in cell performance between the ordered and the disordered mesoporous titania photoanodes. In this regard, the much higher J_{SC} value obtained for the ordered mesoporous titania photoanodes than the disordered ones at $C_{surf} < 6 \times 10^{-8}$ M implies that the ordered film morphology can expedite transport and collection of electrons.

Consequently, the films thicker than ~3.5 μm are improper for exploring and comparing the dependence of the solar cell performance on the mesostructural morphologies because of the blurred difference in structures caused by the presence of macro-cracks. In further studies of the influence of film morphologies on the cell performance, both the ordered and the disordered mesoporous titania films were fixed at 2.5 μm in thickness unless otherwise indicated, because of several features at such thickness: identical roughness factor, identical dye loading, no disturbance from cracks, and big difference in J_{SC} for the purpose of a striking contrast.

Figure 6a is the current−voltage characteristics of the DSSCs derived from the ordered and the disordered mesoporous titania of 2.5 μm thick. Under the standard global AM 1.5 solar condition, the N719-sensitized DSSC made of the ordered mesoporous titania gave $J_{SC} = 8.86$ mA cm^{-2}, $V_{OC} = 0.758$ V, and $FF = 68.0\%$, yielding a 4.56% conversion efficiency. The disordered mesoporous titania solar cell showed $J_{SC} = 6.75$ mA cm^{-2}, $V_{OC} = 0.773$ V, and $FF = 69.2\%$, yielding a 3.61% conversion efficiency.

Figure 6b displays the IPCE of the solar cells made of the ordered and the disordered mesoporous titania of 2.5 μm thick, and the responses were uncorrected for the absorption and scattering of incident light by the substrates. The cell made of the ordered mesoporous titania film exhibited a higher quantum efficiency over the whole spectral range of 400−800 nm than that of its disordered counterpart. The maximum IPCE of the ordered mesoporous titania solar cell was 69% at 520 nm. From the overlap integral of this curve, one calculated a J_{SC} of 8.61 mA cm^{-2}. It is consistent with the current−voltage characterization result of $J_{SC} = 8.86$ mA cm^{-2} for the same cell, indicating that the mismatch factor

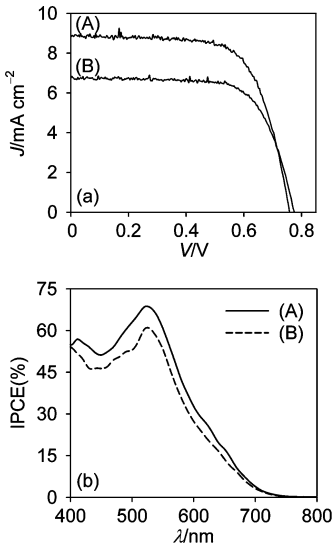

FIGURE 6. (a) Current−voltage, and (b) IPCE curves of the DSSCs made of the (A) ordered and (B) disordered mesoporous 2.5 μm thick titania films.

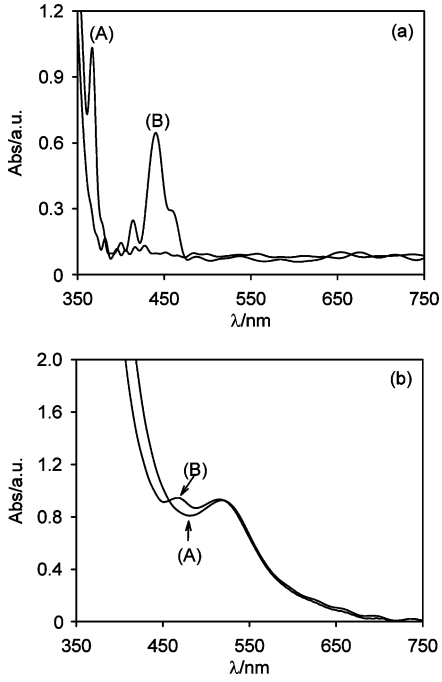

FIGURE 7. (a) UV−vis absorption spectra of the (A) ordered and (B) disordered mesoporous 2.5 μm thick titania films. (b) UV−vis absorption spectra of the corresponding N719-sensitized DSSCs filled with electrolyte. The spectra in (a) refer to FTO substrate. The spectra in (b) refer to one FTO substrate glued to another Pt-coated FTO substrate.

of our solar simulator is close to unity. Likewise, the DSSC made of the disordered mesoporous titania showed IPCE = 61 % at 520 nm and J_{SC} = 7.51 mA cm^{-2}.

The absorption spectra of the mesoporous titania films of different morphologies are shown in Figure 7a. Strikingly, the spectra of the ordered and the disordered films showed an intense absorption band being centered at ~370 and ~440 nm, respectively. According to their FT-IR transmittance spectra (Figure 8), the two bands centered at 3400 and 1640 cm^{-1} are assigned to the stretching vibration of O−H

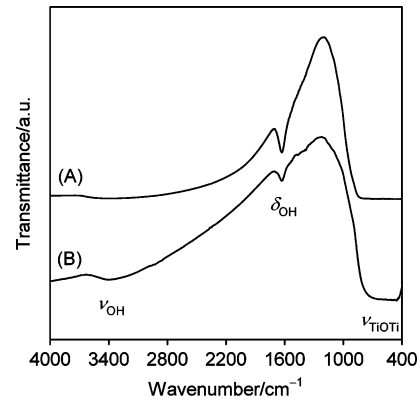

FIGURE 8. FT-IR transmittance spectra of the (A) ordered and (B) disordered mesoporous 2.5 μm thick titania films.

(ν_{OH}) and the bending vibration of H−O−H (δ_{OH}), respectively. They evidence the presence of hydroxyl groups in the inorganic films. The low-frequency band in the range of 900−400 cm^{-1} corresponds to the stretching vibration of Ti−O−Ti (ν_{TiOTi}). There is no band characteristic of organic species, indicating a complete removal of the copolymer templates. Consequently, the intense absorption band observed in Figure 7a could not be caused by any organic remains. It is also not due to the bandgap absorption of titania, which corresponds to the sharp increase in absorption at about 360 nm. It is very likely to originate from the scattering in the mesoporous titania film due to the difference in the refractive indexes between the pore (air) and the titania framework. The discrepancy in pore size, titania nanocrystallite size, and porosity for the ordered and the disordered mesoporous titania films largely determines that the position and intensity of their respective scattering bands are different. This is supported by the fact that the light scattering is greatly reduced by the electrolyte filling, where the refractive index of the electrolyte better matches that of titania than air (Figure 7b) (21). It suggests an insignificant contribution of the scattering effect to the cell performance, especially for the ordered film where the scattering band was located outside the visible light range. The IPCE curves in Figure 6b confirms that there is no oddness caused by this scattering effect. In addition, a broad band peaking at ~520 nm was observed, which is assigned to the metal-to-ligand charge-transfer transition (MLCT) of N719. The intensity of this band is nearly identical for the DSSCs derived from both the ordered and the disordered mesoporous films, being consistent with the fact that the degree of dye loading is irrelative to the morphology of the mesoporous titania.

The above discussion on the dye loading and optical properties suggests that the higher J_{SC} observed for the ordered mesoporous titania photoanodes could only be caused by the superior electron transport ability as compared to the disordered one. Indeed, it has been reported that electrons pass through a chain of spherical grains by diffusion in the conduction band of titania, punctuated by a series of trapping and detrapping events (10, 22, 23). The grain connectivity, the trap density, location, and depth all affect the electron transport (23). For instance, the trap depth affects the transport rate, because if the traps are shallow,

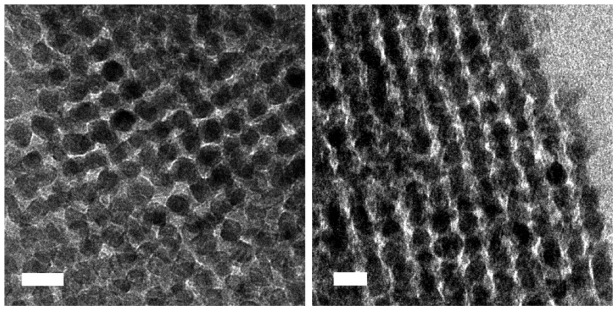

FIGURE 9. TEM images of the ordered mesoporous 2.5 μm thick titania film. Scale bar: 20 nm.

the electrons detrap much faster (23). Considering the identical fabrication protocol and comparable trap features for both the ordered and disordered film mesostructures in the present study, the neck connections between grains that provide pathways for electron transport shall have a noticeable effect on the photocurrent. As shown by TEM studies (Figure 9) of the ordered mesoporous titania film, the titania nanoparticles, where one nanoparticle consists of one crystalline grain, are packed rather orderly with clear contact area between the grains. This regularly geometrical arrangement of the titania skeleton expedites electron transport in the conduction band of the ordered mesoporous titania. Further characterization using impedance is under way in order to better understand the charge transport and recombination behaviors in supramolecular templated mesoporous titania systems.

4. CONCLUSIONS

Supramolecular templating in combination with the layer-by-layer deposition has been successfully developed to synthesize thick mesoporous titania films of two different morphologies and varying thicknesses, namely ordered body-centered orthorhombic and disordered wormlike mesostructure, for application in DSSCs. Relatively high efficiencies (6−7%) were successfully achieved for the mesoporous films of 5−6 μm in thickness, undoubtedly among the highest achieved for the DSSCs made of mesoporous titania thick films. The mesoporous film morphology is shown to be a key parameter in determining their effectiveness in DSSC device applications. The ordered mesoporous titania film showed an enhanced solar energy conversion efficiency than that of the disordered counterpart, as a result of the enhancement in photocurrent. Both the ordered and the disordered films of the same thickness demonstrate comparable degrees of accessible area in the actual device geometry for dye uptake. A strong optical scattering band was observed for both the ordered and the disordered mesoporous films, because of the difference in refractive indexes between the mesopore and the titania framework. However, light scattering was greatly reduced by the electrolyte filling and thus contributes less to the cell performance. The better organized geometrical morphology of titania skeleton with grain connectivity in the ordered titania film is beneficial to the electron transport. Nevertheless, the dependence of the cell performance on mesostructural morphology is weakened when the film thickness was above ~3.5 μm, because of the serious film cracks, which deteriorate the long-range mesostructural ordering.

Acknowledgment. This paper is based upon work supported by the Science and Engineering Research Council − A*Star, Singapore, under Grant No. 072 101 0013. Authors also acknowledge the support of the National University of Singapore.

REFERENCES AND NOTES

(1) O'Regan, B.; Grätzel, M. *Nature* **1991**, *353*, 737–740.
(2) Grätzel, M. *Nature* **2001**, *414*, 338.
(3) Nazeeruddin, M. K.; Péchy, P.; Renouard, T.; Zakeeruddin, S. M.; Humphry-Baker, R.; Comte, P.; Liska, P.; Cevey, L.; Costa, E.; Shklover, V.; Spiccia, L.; Deacon, G. B.; Bignozzi, C. A.; Grätzel, M. *J. Am. Chem. Soc.* **2001**, *123*, 1613–1624.
(4) Grätzel, M. *Inorg. Chem.* **2005**, *44*, 6841–6851.
(5) Grätzel, M. *Prog. Photovolt.* **2000**, *8*, 171–185.
(6) Fthenakis, V. M.; Moskowitz, P. D. *Prog. Photovolt. Res. Appl.* **2000**, *8*, 27–38.
(7) Kim, Y. J.; Lee, Y. H.; Lee, M. H.; Kim, H. J.; Pan, J. H.; Lim, G. I.; Choi, Y. S.; Kim, K.; Park, N.; Lee, C.; Lee, W. I. *Langmuir* **2008**, *24*, 13225–13230.
(8) Paulose, M.; Shankar, K.; Varghese, O. K.; Mor, G. K.; Grimes, C. A. *J. Phys. D: Appl. Phys.* **2006**, *39*, 2498–2503.
(9) Zhang, Q.; Chou, T. P.; Russo, B.; Jenekhe, S. A.; Cao, G. *Angew. Chem., Int. Ed.* **2008**, *47*, 2402–2406.
(10) Crossland, E. J. W.; Nedelcu, M.; Ducati, C.; Ludwigs, S.; Hillmyer, M. A.; Steiner, U.; H; Snaith, J. *Nano. Lett.* **2009**, *9*, 2813–2819.
(11) Wang, Y. Q.; Chen, S. G.; Tang, X. H.; Palchik, O.; Zaban, A.; Koltypin, Y.; Gedanken, A. *J. Mater. Chem.* **2001**, *11*, 521–526.
(12) Hou, K.; Tian, B.; Li, F.; Bian, Z.; Zhao, D.; Huang, C. *J. Mater. Chem.* **2005**, *15*, 2414–2420.
(13) Kartini, I.; Menzies, D.; Blake, D.; da Costa, J. C. D.; Meredith, P.; Riches, J. D.; Lu, G. Q. *J. Mater. Chem.* **2004**, *14*, 2917–2921.
(14) Procházka, J.; Kavan, L.; Zukalova, M.; Frank, O.; Kalbáč, M.; Zukal, A.; Klementová, M.; Carbone, D.; Graetzel, M. *Chem. Mater.* **2009**, *21*, 1457–1464.
(15) Zukalová, M.; Zukal, A.; Kavan, L.; Nazeeruddin, M. K.; Liska, P.; Grältzel, M. *Nano Lett.* **2005**, *5*, 1789–1792.
(16) Procházka, J.; Kavan, L.; Shklover, V.; Zukalová, M.; Frank, O.; Kalbáč, M.; Zukal, A.; Pelouchová, H.; Janda, P.; Mocek, K.; Klementová, M.; Carbone, D. *Chem. Mater.* **2008**, *20*, 2985–2993.
(17) Zhang, Y.; Sim, C. H.; Yuwono, A. H.; Li, J.; Wang, J. *J. Am. Ceram. Soc.* **2009**, *92*, 1317–1321.
(18) Ito, S.; Liska, P.; Comte, P.; Charvet, R.; Péchy, P.; Bach, U.; Schmidt-Mende, L.; Zakeeruddin, S. M.; Kay, A.; Nazeeruddin, M. K.; Grätzel, M. *Chem. Commun.* **2005**, 4351–4353.
(19) Neale, N. R.; Kopidakis, N.; Lagemaat, J.; Grältzel, M.; Frank, A. J. *J. Phys. Chem. B* **2005**, *109*, 23183–23189.
(20) Cass, M. J.; Walker, A. B.; Martinez, D.; Peter, L. M. *J. Phys. Chem. B* **2005**, *109*, 5100–5107.
(21) Ito, S.; Nazeeruddin, M. K.; Liska, P.; Comte, P.; Charvet, R.; Péchy, P.; Jirousek, M.; Kay, A.; Zakeeruddin, S. M.; Grätzel, M. *Prog. Photovolt: Res. Appl.* **2006**, *14*, 589–601.
(22) Wang, Q.; Ito, S.; Grätzel, M.; Fabregat-Santiago, F.; Mora-Seró, I.; Bisquert, J.; Bessho, T.; Imai, H. *J. Phys. Chem. B* **2006**, *110*, 25210–25221.
(23) Cass, M. J.; Qiu, F. L.; Walker, A. B.; Fisher, A. C.; Peter, L. M. *J. Phys. Chem. B* **2003**, *107*, 113–119.

AM900529E